

A 3-D Wideband Multi-Confocal Ellipsoid Model for Wireless Massive MIMO Communication Channels with Uniform Planar Antenna Array

Lu Bai¹, Cheng-Xiang Wang^{2, 1}, Shangbin Wu³, Jian Sun^{1, 4}, Wensheng Zhang¹

¹Shandong Provincial Key Lab. of Wireless Communications, Shandong University, Shandong, 250100, China.

²School of Engineering and Physical Sciences, Heriot-Watt University, Edinburgh, EH14 4AS, UK.

³Samsung R&D Institute UK, Staines-upon-Thames, TW18 4QE, UK.

⁴State Key Lab. of Millimeter Waves, Southeast University, Nanjing, 210096, P.R.China.

Email: bailusdu@126.com, cheng-xiang.wang@hw.ac.uk, shangbin.wu@samsung.com, {sunjian, zhangwsh}@sdu.edu.cn

Abstract—This paper first proposes a three dimensional (3-D) non-stationary wideband multi-confocal ellipsoid channel model with uniform planar antenna array (UPA) for massive multiple-input multiple-output (MIMO) wireless communication systems. The proposed 3-D geometry-based stochastic model (GBSM) not only considers the non-stationary channel characteristics in time domain but also describes the non-stationary channel characteristics in array domain by adopting a birth-death (BD) process and seed algorithm on UPA for the first time. At the meanwhile, selective cluster evolution and cluster evolution areas (CEAs) are first proposed in this paper. Only clusters in CEAs go through cluster evolution because near-field effect and other clusters can be observed by all antennas. Channel parameters, including delay, Doppler frequency, angle of departure (AoD), and angle of arrive (AoA), are considered in both the azimuth direction and elevation direction. This paper also considers rotations of UPAs. Based on the proposed theoretical reference model, the relevant simulation model is also obtained. The statistical properties of theoretical reference model and simulation model can match well with numerical results.

Keywords – Non-stationary, wideband, multi-confocal ellipsoid, massive MIMO, GBSM, CEA, 3-D model, seed algorithm, UPA.

I. INTRODUCTION

Recently, massive MIMO technology has been widely and generally recognized as one of the most important technologies of the fifth generation (5G) wireless communication networks. It can meet the requirements of the 5G wireless communication systems by achieving a better signal-to-noise ratio (SNR) through sharpening directional transmission largely, mitigating multipath fading because of spatial diversity substantially and increasing the channel capacity because of spatial multiplexing [1–3].

For massive MIMO wireless communication systems design and performance evaluation, it is necessary to get an accurate, general, and easy-to-use model to describe the underlying realistic propagation channels. Compared with conventional MIMO technology, not only massive MIMO communication systems are equipped with tens or even hundreds of antennas, but also massive

MIMO channel has its unique channel characteristics, such as spherical wavefront propagation [4], non-stationary channel characteristics in time and array domain [5] which should be modeled in massive MIMO channel model and decreasing correlation of channel impulse responses (CIRs) [6].

Up to now, there are lots of massive MIMO channel models [7]. Kronecker model in [8] is a massive MIMO correlation-based stochastic model (CBSM). It models non-stationary effects along the array by Markov BD processes and improves capacity estimation. The proposed massive MIMO channel models in [9–13] are all GBSMs. The authors in [9] developed a non-stationary wideband multi-confocal ellipse channel model for massive MIMO communication systems. In [11], the authors proposed a non-stationary channel model where clusters are located on the concentric multi-ring. In [13], authors came up with a 3-D wideband twin-cluster channel model whose parameters follow certain distributions, including delay, Doppler frequency, AoD, AoA and so on. In these three models, they considered spherical wavefronts and used a BD process to model non-stationary channel characteristics in both array and time domains. The model in [10] is a 3-D regular shape geometry-based stochastic model (RS-GBSM) based on double cylinders. In [12], visibility regions (VRs) where a cluster can be observed by the moving station (MS) were extended to the base station (BS) array for capturing non-stationary properties in array domain.

Compared to 2-D models [8], [10], [11], 3-D models [10], [13] are able to capture channel characteristics in the elevation direction. The 3-D double cylinders model in [10] claimed that it considered elevation angles, but the scatterers located on the double cylinders did not have the identical delays and the complexity of the channel model increases, which violates the advantage of elliptic models for wideband channels. The model in [13] focused on the relationship between parameters and scatters instead of the scatters themselves. At the meanwhile, all above models only consider uniform linear antenna array (ULA). However, UPAs

have been widely used in massive MIMO systems for saving spatial resource. To overcome above problems, this paper proposes a novel 3-D theoretical non-stationary wideband multi-confocal ellipsoid massive MIMO channel model with UPA and selective cluster evolution, which is able to model clusters with identical delays on the same ellipsoid while different ellipsoids represent wideband channel characteristic. Also, channel parameters in elevation direction and rotations of UPA are taken into account.

The remainder of this paper is organized as follows. Section II describes the 3-D theoretical wideband multi-confocal ellipsoid model. The statistical properties of the proposed reference model are obtained in Section III. Section IV presents the relevant simulation model. The results and analysis are given in Section V. At last, the conclusions are drawn in Section VI.

II. THEORETICAL REFERENCE MODEL

In the theoretical reference model shown in Fig.1, each ellipsoid is the rotation of an ellipse with respect to the y axis. The o -th cluster of scatters is located on the o -th ellipsoid with major axis $2a_o$. The Tx and Rx are equipped with UPAs with M_T (m row \times n column) and M_R (p row \times q column) omnidirectional antennas, respectively. The central points of UPAs are located at the focal points of the confocal ellipsoids with major axis $2f$. The antenna spacings of the Tx and Rx are δ_T and δ_R , respectively. Note that \mathbf{A}_{uw}^T (\mathbf{A}_{lk}^R) represents the vector of the $u(l)$ -th row and $w(k)$ -th column antenna in transmit (receiver) antenna array. \mathbf{A}_{uw}^T (\mathbf{A}_{lk}^R) represents the $u(l)$ -th row and $w(k)$ -th column antenna in transmit (receiver) antenna array.

The coordinates of antennas in the global coordinate system (GCS) and local coordinate system (LCS) are different. The scattering environment is defined in the GCS. The LCS is defined for UPAs of Tx and Rx.

In the LCS, the antenna vector in the Tx is $\mathbf{A}'_{uw}^T = [x'_{uw}^T, y'_{uw}^T, z'_{uw}^T]^T$, while the antenna vector in the Rx is $\mathbf{A}'_{lk}^R = [x'_{lk}^R, y'_{lk}^R, z'_{lk}^R]^T$, where

$$x'_{uw}^T = \begin{cases} -\frac{m-2u+1}{2}\delta_T, & u < \frac{m+1}{2}, \\ \frac{m-2u+1}{2}\delta_T, & u \geq \frac{m+1}{2} \end{cases} \quad (1)$$

$$y'_{uw}^T = \begin{cases} -\frac{n-2w+1}{2}\delta_T, & w < \frac{n+1}{2}, \\ \frac{n-2w+1}{2}\delta_T, & w \geq \frac{n+1}{2} \end{cases} \quad (2)$$

$$z'_{uw}^T = 0 \quad (3)$$

$$x'_{lk}^R = \begin{cases} -\frac{p-2l+1}{2}\delta_R, & l < \frac{p+1}{2}, \\ \frac{p-2l+1}{2}\delta_R, & l \geq \frac{p+1}{2} \end{cases} \quad (4)$$

$$y'_{lk}^R = \begin{cases} -\frac{q-2k+1}{2}\delta_R, & k < \frac{q+1}{2}, \\ \frac{q-2k+1}{2}\delta_R, & k \geq \frac{q+1}{2} \end{cases} \quad (5)$$

$$z'_{lk}^R = 0. \quad (6)$$

The placement of the UPAs in the GCS is defined by the transformation from the GCS to the LCS. We describe an arbitrary 3-D rotation of the LCS with respect to the GCS by the angles α , β , and γ . The orientation of the UPAs with respect to the GCS is defined by a sequence of rotations in [14]. Note that

$$\mathbf{A}_{uw}^T = \mathbf{R} \mathbf{A}'_{uw}^T \quad (7)$$

$$\mathbf{A}_{lk}^R = \mathbf{R} \mathbf{A}'_{lk}^R \quad (8)$$

$$\mathbf{R} = \mathbf{R}_Z(\alpha) \mathbf{R}_Y(\beta) \mathbf{R}_X(\gamma) = \begin{pmatrix} +\cos\alpha & -\sin\alpha & 0 \\ +\sin\alpha & -\cos\alpha & 0 \\ 0 & 0 & 1 \end{pmatrix} \begin{pmatrix} +\cos\beta & 0 & -\sin\beta \\ 0 & 1 & 0 \\ -\sin\beta & 0 & +\cos\beta \end{pmatrix} \begin{pmatrix} 1 & 0 & 0 \\ 0 & +\cos\gamma & -\sin\gamma \\ 0 & +\sin\gamma & +\cos\gamma \end{pmatrix}. \quad (9)$$

In massive MIMO channel models, non-stationary channel characteristics in array domain and spherical wavefront should be considered because of near-field effect while Rayleigh distance increases with the dimension of antenna array [9–13]. But, all these papers did not distinguish the near-field of antenna array. They consider non-stationary channel characteristics on the array and spherical wavefront in any case, whatever the relationship between Rayleigh distance and the distance between Tx and Rx. The near-field effects are valid only in the area which radius is Rayleigh distance [15]. So, this paper first defines the threshold of the cluster evolution as Γ , which is the radius of CEA. Note that

$$\Gamma_T = \frac{2\delta_T^2 (m^2 + n^2)}{\lambda} \quad (10)$$

$$\Gamma_R = \frac{2\delta_R^2 (p^2 + q^2)}{\lambda}. \quad (11)$$

The red line spheres in Fig.1 whose radius are Γ_T and Γ_R respectively is the CEA where clusters can be only affected by part of the antennas. So, as we can see in Fig.1, Cluster₁ Cluster _{o} and Cluster _{N} are all in the CEA of transmitter and they are non-stationary on the transmitter planar antenna array. After BD process on the antenna array, Cluster _{o} can effect A_{uw}^T but Cluster₁ Cluster _{N} can not. In a similar way, Cluster₁ Cluster _{o} and Cluster _{N} are not in the CEA of receiver. They are stationary on the receiver planar antenna array and they can affect all of the antennas in receiver antenna array.

Let N denotes the total number of clusters which may affect the channel in the environment. The algorithm flowchart of array-time evolution of the proposed model is in Fig.8. The part in the red line is the judgement of the CEA and cluster evolution of transmitter, which should be done again for receiver again. The survival probabilities of the clusters on UPAs at the transmitter P_{survival}^T and the receiver P_{survival}^R in BD process can be modeled as exponential functions [13], where

$$P_{\text{survival}}^T = e^{-\lambda \frac{\delta_T}{D_s}} \quad (12)$$

$$P_{\text{survival}}^R = e^{-\lambda \frac{\delta_R}{D_s}}. \quad (13)$$

The definitions of the key parameters in the proposed 3-D theoretical massive MIMO channel model are given in Table I.

The massive MIMO CIR can be characterized by an $M_R \times M_T [(p \times q) \times (m \times n)]$ complex matrix [16], [17]. Note that

$$\mathbf{H}(t, \tau) = \begin{bmatrix} \mathbf{h}_{1,1} & \mathbf{h}_{1,2} & \cdots & \mathbf{h}_{1,m} \\ \mathbf{h}_{2,1} & \mathbf{h}_{2,2} & \cdots & \mathbf{h}_{2,m} \\ \vdots & \vdots & \ddots & \vdots \\ \mathbf{h}_{p,1} & \mathbf{h}_{p,2} & \cdots & \mathbf{h}_{p,m} \end{bmatrix} \quad (14)$$

where

$$\mathbf{h}_{l,u} = \begin{bmatrix} h_{l1,u1} & h_{l1,u2} & \cdots & h_{l1,un} \\ h_{l2,u1} & h_{l2,u2} & \cdots & h_{l2,un} \\ \vdots & \vdots & \ddots & \vdots \\ h_{lq,u1} & h_{lq,u2} & \cdots & h_{lq,un} \end{bmatrix} \quad (15)$$

where $u = 1, 2, \dots, m$, $w = 1, 2, \dots, n$, $l = 1, 2, \dots, p$ and $k = 1, 2, \dots, q$. Next, let us assume that the LOS component only exists for the first ellipsoid and the mean power of the o -th cluster is P_o . The multipath complex gains $h_{lk,uw}(t, \tau)$ of the theoretical model ($S \rightarrow \infty$) between A_{uw}^T and A_{lk}^T at delay τ can be presented as

$$h_{lk,uw}(t, \tau) = \sum_{o=1}^N h_{lk,ij,o}(t) \delta(\tau - \tau_o(t)) \quad (16)$$

- if Cluster _{o} $\in (C_{uw}^T \cap C_{lk}^R)$

$$h_{lk,uw,o}(t) = \underbrace{\delta(o-1) \sqrt{\frac{K}{K+1}} e^{j(2\pi f_{lk,uw}^{\text{LOS}}(t)t + \phi_{lk,uw}^{\text{LOS}}(t))}}_{\text{LOS}} + \underbrace{\sqrt{\frac{P_o}{K+1}} \lim_{S \rightarrow \infty} \left(\frac{1}{\sqrt{S}} \sum_{s=1}^S e^{j(2\pi f_{o,s}(t)t + \phi_{lk,uw,o,s}(t))} \right)}_{\text{NLOS}} \quad (17)$$

- if Cluster _{o} $\notin (C_{uw}^T \cap C_{lk}^R)$

$$h_{lk,uw,o}(t) = 0. \quad (18)$$

A. For the LOS component

The Doppler frequency of A_{lk}^R from $A_{uw}^T, f_{lk,uw}^{\text{LOS}}(t)$ is expressed as

$$f_{lk,uw}^{\text{LOS}}(t) = f_{\max} \frac{\langle \mathbf{D}_{lk,uw}^{\text{LOS}}(t), \mathbf{v}(t) - \mathbf{v}_o(t) \rangle}{\|\mathbf{D}_{lk,uw}^{\text{LOS}}(t)\| \|\mathbf{v}(t) - \mathbf{v}_o(t)\|}. \quad (19)$$

The received phase of A_{lk}^R from A_{uw}^T can be expressed as

$$\phi_{lk,uw}^{\text{LOS}}(t) = \phi_0 + \frac{2\pi}{\lambda} \|\mathbf{D}_{lk,uw}^{\text{LOS}}(t)\| \quad (20)$$

where the distance between A_{uw}^T and A_{lk}^R can be computed by the antenna vector $\mathbf{A}_{uw}^T(t), \mathbf{A}_{lk}^R(t)$, and the distance between the Tx and Rx along the y axis \mathbf{D} , i.e.,

$$\mathbf{D}_{lk,ij}^{\text{LOS}}(t) = \mathbf{D}_{lk,0}^{\text{LOS}}(t) - \mathbf{A}_{uw}^T \quad (21)$$

$$\mathbf{D}_{lk,0}^{\text{LOS}}(t) = \mathbf{D}(t) + \mathbf{A}_{lk}^R. \quad (22)$$

B. For the NLOS component

The Doppler frequency of the Rx via the s -th ray of the o -th cluster $f_{o,s}(t)$ can be expressed as

$$f_{o,s}(t) = f_{\max} \frac{\langle \mathbf{D}_{o,s}^R(t), \mathbf{v}(t) - \mathbf{v}_o(t) \rangle}{\|\mathbf{D}_{o,s}^R(t)\| \|\mathbf{v}(t) - \mathbf{v}_o(t)\|}. \quad (23)$$

Similar to the LOS component, the received phase of the Rx via the s -th ray of the o -th cluster $f_{o,s}(t)$ can be computed as

$$\phi_{lk,uw,o,s}(t) = \phi_0 + \frac{2\pi}{\lambda} (\|\mathbf{D}_{lk,o,s}^R(t)\| + \|\mathbf{D}_{uw,o,s}^T(t)\|) \quad (24)$$

where the absolute distance between the Tx and Rx via the s -th ray of the o -th cluster can be derived according to their geometrical relationships:

$$\|\mathbf{D}_{o,s}^R(t)\| = \frac{2a_o \sin \alpha_{o,s}^T}{\sin \alpha_{o,s}^T + \sin(\pi - \alpha_{o,s}^R)}. \quad (25)$$

As a result, we can get the distance vector and the angle relationships:

$$\mathbf{D}_{o,s}^R(t) = \|\mathbf{D}_{o,s}^R(t)\| \begin{pmatrix} \cos \psi_{o,s}^R(t) \cos \theta_{o,s}^R(t) \\ \sin \psi_{o,s}^R(t) \cos \theta_{o,s}^R(t) \\ \sin \theta_{o,s}^R(t) \end{pmatrix}. \quad (26)$$

Based on the above equations, we can get

$$\mathbf{D}_{lk,o,s}^R(t) = \mathbf{D}_{o,s}^R(t) - \mathbf{A}_{lk}^R \quad (27)$$

$$\mathbf{D}_{uw,o,s}^T(t) = \mathbf{D}_{o,s}^T(t) - \mathbf{A}_{uw}^T \quad (28)$$

$$\mathbf{D}_{o,s}^T(t) = \mathbf{D}(t) - \mathbf{D}_{o,s}^R(t) \quad (29)$$

$$\alpha_{o,s}^R = \arccos(\cos\theta_{o,s}^R \times \sin\psi_{o,s}^R). \quad (30)$$

For the NLOS components, AoAs $\alpha_{o,s}^R$ and AoDs $\alpha_{o,s}^T$ are not independent in an ellipsoid model. Their relationship can be expressed as

$$\alpha_{o,s}^T = \begin{cases} g(\alpha_{o,s}^R) & \text{if } 0 < \alpha_{o,s}^R \leq \alpha_0 \\ g(\alpha_{o,s}^R) + \pi & \text{if } \alpha_0 < \alpha_{o,s}^R \leq 2\pi - \alpha_0 \\ g(\alpha_{o,s}^R) + 2\pi & \text{if } 2\pi - \alpha_0 < \alpha_{o,s}^R \leq 2\pi \end{cases} \quad (31)$$

$$g(\alpha_{o,s}^R) = \arctan\left(\frac{(k_0^2 - 1)\sin\alpha_{o,s}^R}{2k_0 + (k_0^2 + 1)\cos\alpha_{o,s}^R}\right) \quad (32)$$

$$\alpha_0 = \pi - \arctan\left(\frac{k_0^2 - 1}{2k_0}\right) \quad (33)$$

$$k_0 = \frac{a_o}{f}. \quad (34)$$

Given the semi-major axis f of the first ellipsoid, a_o can be determined by $\tau_o(t)$ relative to the first ellipsoid as

$$a_o(t) = c\tau_o(t) + a_1 \quad (35)$$

where c is the speed of light. The delay of the o -th cluster is assumed to be the sum of two components, i.e.,

$$\tau_o(t) = \frac{\|\mathbf{D}_{o,s}^R(t)\| + \|\mathbf{D}_{o,s}^T(t)\|}{c}. \quad (36)$$

III. STATISTIC PROPERTIES

In this section, we will derive the corresponding statistical properties of wideband multi-confocal ellipsoid model.

A. Spatial-Temporal Correlation Function

The spatial-temporal correlation function between the channel gains $h_{lk,uw,c}(t)$ and $h_{l'k',u'w',o}(t)$ is defined as

$$\rho_{lk,uw,l'k',u'w',o}(\delta_T, \delta_R, \Delta t; t) = \mathbf{E}\left[\frac{h_{lk,uw,o}^*(t)h_{l'k',u'w',o}(t + \Delta t)}{|h_{lk,uw,o}^*(t)||h_{l'k',u'w',o}(t + \Delta t)|}\right]. \quad (37)$$

When the LOS component and NLOS components are independent, it can be rewritten as

$$\begin{aligned} & \rho_{lk,uw,l'k',u'w',o}(\delta_T, \delta_R, \Delta t; t) \\ &= \rho_{lk,uw,l'k',u'w',o}^{\text{LOS}}(\delta_T, \delta_R, \Delta t; t) + \rho_{lk,uw,l'k',u'w',o}^{\text{NLOS}}(\delta_T, \delta_R, \Delta t; t) \end{aligned} \quad (38)$$

where

$$\begin{aligned} & \rho_{lk,uw,l'k',u'w',o}^{\text{LOS}}(\delta_T, \delta_R, \Delta t; t) = \frac{K\delta(o-1)}{K+1} \\ & e^{j[2\pi f_{l'k',u'w'}^{\text{LOS}}(t+\Delta t)(t+\Delta t) - 2\pi f_{lk,uw}^{\text{LOS}}(t)(t) + \phi_{l'k',u'w'}^{\text{LOS}}(t+\Delta t) - \phi_{lk,uw}^{\text{LOS}}(t)]} \end{aligned} \quad (39)$$

$$= \frac{1}{K\delta(o-1)+1} \mathbf{E}\left[\lim_{S \rightarrow \infty} \left(\frac{1}{\sqrt{S}} \sum_{s=1}^S e^{j\Phi_0}\right)\right] \quad (40)$$

with

$$\begin{aligned} \Phi_0 = & 2\pi f_{o,s}(t + \Delta t)(t + \Delta t) - 2\pi f_{o,s}(t)(t) \\ & + \phi_{l'k',u'w',o,s}(t + \Delta t) - \phi_{lk,uw,o,s}(t). \end{aligned} \quad (41)$$

B. Spatial Cross-Correlation Function

The spatial cross-correlation function (CCF) $\rho_{lk,uw,l'k',u'w',o}(\delta_T, \delta_R; t)$ can be obtained from the spatial-temporal correlation function by setting $\Delta t = 0$, i.e.,

$$\rho_{lk,uw,l'k',u'w',o}(\delta_T, \delta_R; t) = \mathbf{E}\left[\frac{h_{lk,uw,o}^*(t)h_{l'k',u'w',o}(t)}{|h_{lk,uw,o}^*(t)||h_{l'k',u'w',o}(t)|}\right]. \quad (42)$$

C. Temporal Auto-Correlation Function

By setting $u = u'$, $w = w'$ and $l = l'$, $k = k'$, the spatial-temporal correlation function reduces to the temporal auto-correlation function (ACF) $\rho_{lk,uw,o}(\Delta t; t)$, i.e.,

$$\rho_{lk,uw,o}(\Delta t; t) = \mathbf{E}\left[\frac{h_{lk,uw,o}^*(t)h_{lk,uw,o}(t + \Delta t)}{|h_{lk,uw,o}^*(t)||h_{lk,uw,o}(t + \Delta t)|}\right]. \quad (43)$$

IV. SIMULATION MODEL

The number of clusters in this theoretical reference channel model is assumed to be infinity ($S \rightarrow \infty$). However, a actual number of clusters in a channel simulator is finite to trade off accuracy and complexity. In this section, we will obtain a channel simulator with a finite and suitable number of clusters to present channel characteristics as accurately as possible. Thus, the massive MIMO simulation channel model is derived as

$$\begin{aligned} h_{lk,uw,o}(t) = & \underbrace{\delta(o-1)\sqrt{\frac{K}{K+1}}e^{j(2\pi f_{lk,uw}^{\text{LOS}}(t)t + \phi_{lk,uw}^{\text{LOS}}(t))}}_{\text{LOS}} \\ & + \underbrace{\sqrt{\frac{P_o}{K+1}}\left(\frac{1}{\sqrt{S}}\sum_{s=1}^S e^{j(2\pi f_{o,s}(t)t + \phi_{lk,uw,o,s}(t))}\right)}_{\text{NLOS}}. \end{aligned} \quad (44)$$

This paper defines the spatial-temporal correlation function $\rho_{lk,uw,l'k',u'w',o}(\delta_T, \delta_R, \Delta t; t)$ with AoAs/AoDs distributed according to the cumulative distribution function (CDF) and we calculate it by the method of equal areas (MEA).

V. RESULTS AND DISCUSSIONS

Fig. 2 and Fig. 3 compare the spatial CCFs and temporal ACFs of the reference model, simulation model, and simulation results, respectively. All the results align well with each other, demonstrating that the derivations and simulations are valid. The distance between A_{23}^R and A_{22}^R is δ_R , which is equal to the distance between A_{32}^R and A_{22}^R . The difference between their spatial CCFs in Fig. 4 shows non-stationarity on array axis according to cluster evolution. In Fig. 5, the x axis is the row index of antenna and the y axis is the column index of antenna. It shows the evolution of different clusters on the UPA. Fig. 6 shows the effects of different UPAs setup with different R . So, the transmission from LCS to GCS is necessary. Fig. 7 shows the comparison of the spatial CCFs with different UPAs in same number of antennas. The Rayleigh distance changes while UPAs change.

VI. CONCLUSIONS

In this paper, we have proposed a novel 3-D theoretical non-stationary wideband multi-confocal ellipsoid channel model with UPA, along with its corresponding simulation model, for massive MIMO wireless communication systems. Selective cluster evolution and seed algorithm in UPA are firstly came up with on non-stationary in array domain. Most importantly, the consistency of channel characteristics between theoretical model and simulation model has been verified in numerical and simulation results.

ACKNOWLEDGEMENT

The authors would like to acknowledge the support from the EU H2020 ITN 5G Wireless project (Grant No. 641985), EU FP7 QUICK project (Grant No. PIRSES-GA-2013-612652), EP-SRC TOUCAN project (Grant No. EP/L020009/1), the National Natural Science Foundation of China (Grant No. 61371110), and Key R&D Program of Shandong Province (Grant No. 2016GX101014).

REFERENCES

- [1] E. G. Larsson, F. Tufvesson, O. Edfors, and T. L. Marzetta, "Massive MIMO for next generation wireless systems," *IEEE Commun. Mag.*, vol. 52, no. 2, pp. 186-195, Feb. 2014.
- [2] F. Rusek et al., "Scaling up MIMO: opportunities and challenges with very-large arrays," *IEEE Signal Process. Mag.*, vol. 30, no. 1, pp. 40-60, Jan. 2012.
- [3] J. Hoydis, K. Hosseini, S. ten Brink, and M. Debbah, "Making smart use of excess antennas: massive MIMO, small cells, TDD," *Bell Labs Tech. J.*, vol. 18, no. 2, pp. 5-21, Sep. 2013.
- [4] J.-S. Jiang and M. A. Ingram, "Spherical-wave model for short-range MIMO," *IEEE Trans. Commun.*, vol. 53, no. 9, pp. 1534-1541, Sep. 2005.
- [5] X. Gao, O. Edfors, F. Tufvesson, and E. G. Larsson, "Massive MIMO in real propagation environments: do all antennas contribute equally?" *IEEE Trans. Commun.*, vol. 63, no. 11, pp. 3917-3928, Nov. 2015.
- [6] J. Hoydis, C. Hoek, T. Wild, and S. ten Brink, "Channel measurements for large antenna arrays," in *Proc. ISWCS'12*, Paris, France, Aug. 2012, pp. 811-815.

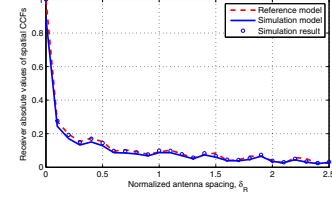


Fig. 2: The comparison of the spatial CCFs between $h_{22,12}$ and $h_{23,12}$ ($M_T = 20 \times 8$, $M_R = 12 \times 12$, $D = 50$ m, $v = 3$ m/s, $\lambda = 0.15$ m, $v_o = 0.5$ m/s, T_0 (intial time)=1 s).

- [7] C.-X. Wang, S. Wu, L. Bai, X. You, J. Wang, and C.-L. I, "Recent advances and future challenges for massive MIMO channel measurements and models," *Sci. China Inf. Sci.*, vol. 59, no. 2, pp. 1-16, Feb. 2016.
- [8] S. Wu, C.-X. Wang, E.-H. Aggoune, M. Alwakeel, "A novel Kronecker-based stochastic model for massive MIMO channels," in *Proc. IEEE/CIC ICCC'15*, Shenzhen, China, Nov. 2015, pp. 53-57.
- [9] S. Wu, C.-X. Wang, H. Haas, e.-H. M. Aggoune, M. M. Alwakeel, and B. Ai, "A non-stationary wideband channel model for massive MIMO communication systems," *IEEE Trans. Wireless Commun.*, vol. 14, no. 3, pp. 1434-1446, 2015.
- [10] Y. Xie, B. Li, X. Zuo, M. Yang, and Z. Yan, "A 3-D geometry-based stochastic model for 5G massive MIMO channels," in *Proc. QSHINE'15*, Aug. 2015, pp. 216-222.
- [11] H. Wu, S. Jin, and X. Gao, "Non-stationary multi-ring channel model for massive MIMO systems," in *Proc. WCSP'15*, Nanjing, China, Oct 2015, pp. 1-6.
- [12] X. Gao, O. Edfors, F. Rusek, and F. Tufvesson, "Linear pre-coding performance in measured very-large MIMO channels," in *Proc. IEEE VTC'11-Fall*, San Francisco, CA, USA, Sept. 2011, pp. 1-5.
- [13] S. Wu, C. X. Wang, E. H. M. Aggoune, M. M. Alwakeel, and Y. He, "A non-stationary 3-D wideband twin-cluster model for 5G massive MIMO channels," *IEEE J. Select. Areas Commun.*, vol. 32, no. 6, pp. 1207-1218, 2014.
- [14] 3GPP T.R. 38.900, *Study on channel model for frequency spectrum above 6 GHz*, V14.1.0, 2016.9.
- [15] A. Yaghjw, "An overview of near-field antenna measurements," *IEEE Trans. Antennas Propag.*, vol. AP-34, no. 1, Jan. 1986.
- [16] A. Paulraj, R. Nabar, and D. Gore, *Introduction to space-time wireless communications*, Cambridge University Press, Cambridge, 2008.
- [17] T. Zwick, C. Fischer, D. Didascalou, and W. Wiesbeck, "A stochastic spatial channel model based on wave-propagation modeling," *IEEE J. Sel. Areas Commun.*, vol. 18, no. 1, pp. 6-15, Jan. 2000.

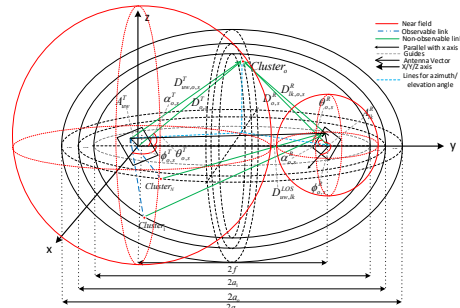


Fig. 1: A 3-D wideband multi-confocal ellipsoid model for massive MIMO communication channels.

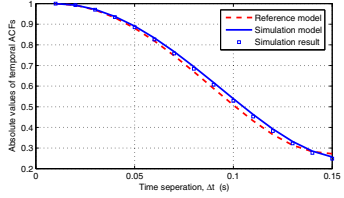


Fig. 3: The comparison of the temporal ACFs of $h_{22,12}$, ($M_T = 20 \times 8$, $M_R = 12 \times 12$, $D = 50$ m, $v = 3t + 3$ m/s, $\lambda = 0.15$ m, $v_o = 0.5$ m/s, T_0 (intial time)=1 s).

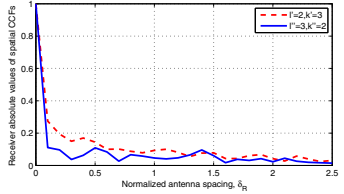


Fig. 4: The comparison of the spatial CCFs between $h_{23,12}$, $h_{32,12}$ and $h_{22,12}$ ($M_T = 20 \times 8$, $M_R = 12 \times 12$, $D = 50$ m, $v = 6$ m/s, $\lambda = 0.15$ m, $v_o = 0.5$ m/s, T_0 (intial time)=1 s).

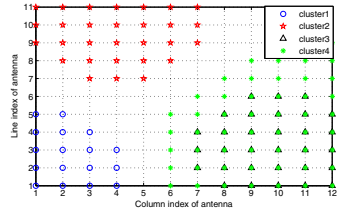


Fig. 5: The evolution of difference cluster on the antenna array

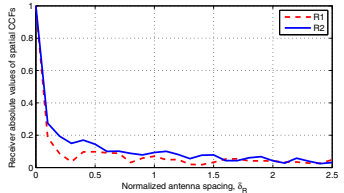


Fig. 6: The comparison of the spatial CCFs between $h_{22,12}$ and $h_{23,12}$ in different \mathbf{R} ($M_T = 20 \times 8$, $M_R = 12 \times 12$, $D = 50$ m, $v = 6$ m/s, $\lambda = 0.15$ m, $v_o = 0.5$ m/s, T_0 (intial time)=1 s, $\alpha = \pi/3$, $\beta = \pi/4$, $\gamma = \pi/3$, $\alpha' = \pi/3$, $\beta' = \pi/4$, $\gamma' = \pi/3$).

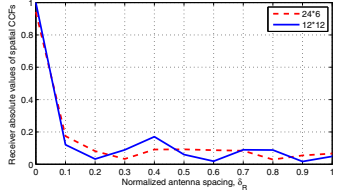


Fig. 7: The comparison of the spatial CCFs between $h_{22,12}$ and $h_{23,12}$ with same number of antennas in different Rayleigh distance ($M_T = 24 \times 6$, $M'_T = 12 \times 12$, $M_R = 12 \times 12$, $R_1 = 134.98$ m, $R_2 = 94.28$ m, $D = 50$ m, $v = 3$ m/s, $\lambda = 0.15$ m, $v_o = 0$ m/s, T_0 (intial time)=1 s).

TABLE I: Summary of key parameter definitions.

Symbol	Definition
\mathbf{v}	velocity vector of the receiver antenna array
\mathbf{v}_o	velocity vector of the o -th cluster
f_{\max}, λ	maximum Doppler frequency and carrier wavelength
$\mathbf{D}_{lk,uw}^{\text{LOS}}$	vector of LOS path from A_{uw}^T to A_{lk}^R
$\mathbf{D}_{lk,0}^{\text{LOS}}$	vector of LOS path from the central point of transmitter to A_{lk}^R
$\mathbf{D}_{uw,o,s}^T$	vector from A_{uw}^T to the o -th cluster via the s -th ray within the cluster
$\mathbf{D}_{o,s}^T$	vector from transmitter to the o -th cluster via the s -th ray
$\mathbf{D}_{lk,o,s}^R$	vector from the o -th cluster to A_{lk}^R via the s -th ray within the cluster
$\mathbf{D}_{o,s}^R$	vector from o -th cluster to receiver via the s -th ray
$f_{lk,uw}^{\text{LOS}}$	Doppler frequency of LOS path from A_{uw}^T to A_{lk}^R
$f_{o,s}$	Doppler frequency of the o -th cluster via the s -th ray
$\phi_{lk,uw}^{\text{LOS}}$	phase of LOS path from A_{uw}^T to A_{lk}^R
ϕ_0	initial phase of the signal at the transmitter
P_o	the mean power of the o -th cluster
K/S	LOS Rician factor and number of rays within one cluster
$\phi_{lk,uw,o,s}^T$	phase of the o -th cluster from A_{uw}^T to A_{lk}^R via the s -th ray
$\psi_{o,s}^T$	azimuth angle of AoD (AAoD) from transmitter to o -th cluster via the s -th ray
$\theta_{o,s}^T$	elevation angle of AoD (EAoD) from transmitter to o -th cluster via the s -th ray
$\psi_{o,s}^R$	azimuth angle of AoA (AAoA) from o -th cluster to receiver via the s -th ray
$\theta_{o,s}^R$	elevation angle of AoA (EAoA) from o -th cluster to receiver via the s -th ray
$\alpha_{o,s}^T$	angle of AoD between $D_{o,s}^T$ and y axis from transmitter to o -th cluster via the s -th ray
$\alpha_{o,s}^R$	angle of AoA between $D_{o,s}^R$ and y axis from o -th cluster to receiver via the s -th ray
$\Gamma_T(\Gamma_R)$	threshold of the cluster evolution in transmit (receiver) antenna array
r_o	the radius of antenna set which can be effected by the o -th cluster according to birth rate
$C_{uw}^T (C_{lk}^R)$	the cluster set which can effect A_{uw}^T (A_{lk}^R)
D_s	scenario-dependent correlation factor on the UPAs

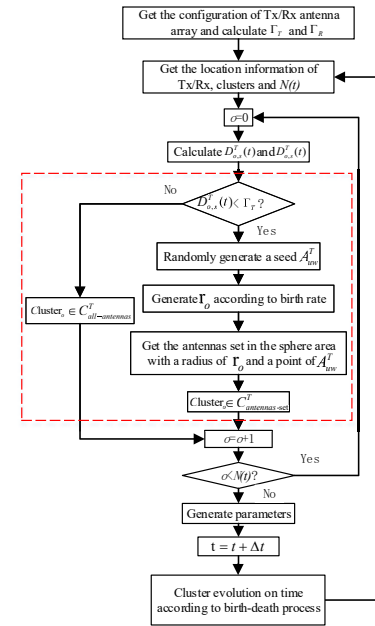


Fig. 8: Algorithm flowchart of array-time evolution of the proposed model.